Materials Horizons

Large-Gain Low-Voltage and Wideband Organic Photodetectors via Unbalanced Charge Transport

Journal:	*Materials Horizons*
Manuscript ID	MH-COM-09-2020-001445.R1
Article Type:	Communication
Date Submitted by the Author:	29-Sep-2020
Complete List of Authors:	Huang, Jianfei; University of California Santa Barbara, Department of Chemistry and Biochemistry Lee, Jaewon; University of California Santa Barbara, Chemistry and Biochemistry, Center for Polymers and Organic Solids; Pohang University of Science and Technology, Department of Chemical Engineering, Center for Advanced Soft Electronics Schrock, Max; University of California Santa Barbara, Chemistry and Biochemistry, Center for Polymers and Organic Solids Dixon, Alana; University of California Santa Barbara, Chemistry and Biochemistry, Center for Polymers and Organic Solids Lill, Alexander; University of California Santa Barbara, Department of Chemistry and Biochemistry Cho, Kilwon; Pohang University of Science and Technology, Chemical Engineering Bazan, Guillermo; University of California, Nguyen, Thuc-Quyen; University of California, Santa Barbara, Chemistry and Biochemistry

New concepts

In the pursuit of highly sensitive photomultiplication organic photodetectors, efficient and versatile photodetection demands high external quantum efficiency (EQE), broadband spectral activity from ultraviolet and visible to infrared region, low operating voltage for safety reasons, and fast response for being applicable in real-time applications. While previous works achieved some of the mentioned criteria, efforts that simultaneously satisfy the full set of mentioned figures-of-merit remain rare and challenging. Unlike the widely employed trap-assisted interfacial band bending mechanism for constructing organic photomultiplication-organic photodiodes, we herein showcase a distinct photoconductive gain mechanism by unbalancing charge transport of electron and holes both in the bulk and at electrode interface of a bulk heterojunction active layer, which brings remarkable EQE over 10^4% at only 1.5 V and response up to 1200 nm. The detector response is fast enough for medical relevant photoplethysmography applications. The work opens a new approach toward comprehensively high-performance large-gain organic photodetectors with external quantum efficiency, broadband response, small operating voltage, and good transient response.

COMMUNICATION

Large-Gain Low-Voltage and Wideband Organic Photodetectors via Unbalanced Charge Transport†

Received 00th January 20xx,
Accepted 00th January 20xx

DOI: 10.1039/x0xx00000x

Jianfei Huang,[a] Jaewon Lee,[b] Max Schrock,[a] Alana L. Dixon,[a] Alexander T. Lill,[a] Kilwon Cho,[c] Guillermo C. Bazan*[d] and Thuc-Quyen Nguyen*[a]

Gain photodetectors offer large photoresponse towards small optical signals. Despite having achieved high external quantum efficiency (EQE), current gain organic photodetectors (OPDs) generally suffer from narrow spectral sensitivity, slow response time and/or large operating voltage for achieving a favorable gain. So far, strategies tackling one of these issues have often come sacrificing another parameter. Here, we present solution-processed all-rounder gain OPDs simultaneously featuring broadband activity (300-1200 nm), low-voltage operation and a fast response speed applicable in real-time heath monitoring. A systematic study shows that the gain mechanism stems from adding a small quantity of tetracyanoquinodimethane (TCNQ), which leads to unbalanced charge transport between holes and electrons. The strategy is also transferrable to other organic bulk heterojunction systems, indicating its promising versatility for further exploration.

Introduction

High-sensitivity photodetectors are widely relevant in optoelectronics, leading to considerable efforts in both fundamental study and applied research.[1–3] Thanks to the progress in materials design, device engineering and understanding of photophysics, photodetectoers based on organic semiconductors are emerging as a promising candidate with favorable cost-effectiveness, large-scale processability, mechanical conformability and flexible tunability.[4–7] Widely applied in organic photovoltaics, the rectifying diode architecture is also heavily employed for constructing OPDs. However, the theoretical EQE of these non-gain OPDs cannot exceed 100%, leading to small outputs when detecting weak signals. This places high demands on external amplification circuitries for practical applications.[8] Alternatively, gain mechanisms can be introduced to construct photomultiplication (PM) photodetectors. Due to the large exciton dissociation energies of disordered organic semiconductors, the established gain mechanisms for inorganic photodetectors, such as ionization impact where one photogenerated charge carrier can induce multiple free charge carriers under large electric field, cannot be readily applied.[9] Instead, other strategies have been explored. For example, by co-depositing inorganic nanoparticles with conjugated polymers, hybrid organic-inorganic photodetectors were demonstrated by Yang and Huang, showing EQE from 10^3% to over 10^5% in the UV and visible spectra.[9,10] The gain mechanism was explained as trap-assisted charge injection. Following this concept, PM OPDs were realized using disproportionate donor-acceptor (D-A) ratios,[11–14] dopant dyes,[15] or by confinement of carriers with extraction barriers.[16] These efforts have led to PM OPDs that compete favorably with avalanche gain inorganic detectors.

However, PM OPDs still face several major challenges. First, their spectral response is limited by poor photon harvesting, and there is insignificant spectral response beyond visible spectra. Efforts have been made to extend the spectral response by incorporating near infrared (NIR) absorbing dyes,[15] conjugated polymers with a narrower bandgap,[11] inorganic quantum dots,[17] or an additional layer with broader spectral absorbance.[18] However, these strategies compromise the EQE achievable without the later introduced spectrum-widening components. Another obstacle is the slow response times from tens of milliseconds to over a second,[8,19] unfavorable for operations involving real-time interactions such as health monitoring. Finally, the voltage required to achieve high photoresponse is still large. The threshold voltage required to achieve over 100% of EQE varies from a few volts to over 10 V, and that for achieving EQE of 10^4 % can be as large as 20

[a] Center for Polymers and Organic Solids, University of California, Santa Barbara, CA 93106, USA
[b] Department of Chemical Engineering and Applied Chemistry, Chungnam National University, Daejeon, 34134, Republic of Korea
[c] Center for Advanced Soft Electronics, Department of Chemical Engineering, Pohang University of Science and Technology, Pohang, 37673, Republic of Korea
[d] Departments of Chemistry and Chemical Engineering, National University of Singapore, Singapore 117543, Republic of Singapore

†Electronic Supplementary Information (ESI) available: Experimental procedures and additional data. See DOI: 10.1039/x0xx00000x

V,[12,14,20,21] which are energy-inefficient and undesirable for the use of OPDs in wearable/portable electronics.

While previous efforts usually show improvement on one of the issues, efforts are scarcely demonstrated to address the composite set of challenges toward comprehensively well performing candidates. Herein, we report a step toward such all-rounder gain OPDs, that simultaneously achieve EQE over 10^4%, wide spectral response cutting off around 1200 nm, real-time monitoring applicable response speed, low gain-threshold voltage of several millivolts, and low operating voltages no larger than that of an AA battery (1.5 V). A systematic study reveals a trap-enhanced photoconductive gain mechanism.[22] The strategy in this work is also applicable to different organic bulk heterojunction (BHJ) systems, making it a promising approach for further exploration with the large diversity of available organic photoactive materials.

Results and discussion

To obtain a wide spectral sensitivity from UV to NIR, a blend of poly[4,8-bis(5-(2-ethylhexyl)thiophen-2-yl)benzo[1,2-b;4,5-b']dithiophene-2,6-diyl-alt-(4-(2-ethylhexyl)-3-fluorothieno[3,4-b]thiophene-)-2-carboxylate-2-6-diyl)] (PTB7-Th) and COTIC-4F was chosen as the active layer for its broadband absorption,[23] with different quantities of TCNQ added into the D-A blend (chemical structures and energy levels shown in Fig. 1a and 1b). Our devices adopt a vertical structure, where the active layer is sandwiched between a poly(3,4-ethylenedioxythiophene) polystyrene sulfonate (PEDOT:PSS) layer and a thermally evaporated Al electrode (Fig. 1c). We refer to the devices with the components of PTB7-Th:COTIC-4F:TCNQ as PC-Tx, where "*x*" represents the weight percentage (*x*%) of TCNQ relative to the total weight of PTB7-Th and COTIC-4F. Due to the solubility limit of TCNQ in chlorobenzene, the largest *x* value in this work is 1.55. For the PC-T0 device, a wide spectral sensitivity from UV to NIR is obtained (Fig. 1d). The EQE increases with the bias, representing a typical effect of facilitated extraction of photogenerated carriers with a stronger electric field. However, due to the inevitable loss in photon capturing, recombination pathways, and the lack of multi-carrier generation processes observed in crystalline inorganic semiconductors,[24,25] the EQE is lower than 100% regardless of the applied large bias. Interestingly, when 1% of TCNQ is introduced for the PC-T1 device, while a similar span of spectral response is observed, the EQE is considerably enhanced to over 10^4% at -1.5 V, indicating the presence of a gain effect (Fig. 1e). Additionally, a small gain-threshold voltage of only -5 mV is required for the EQE to surpass 100%. To investigate the effect of the quantity of TCNQ on photoresponse, the EQE profiles of

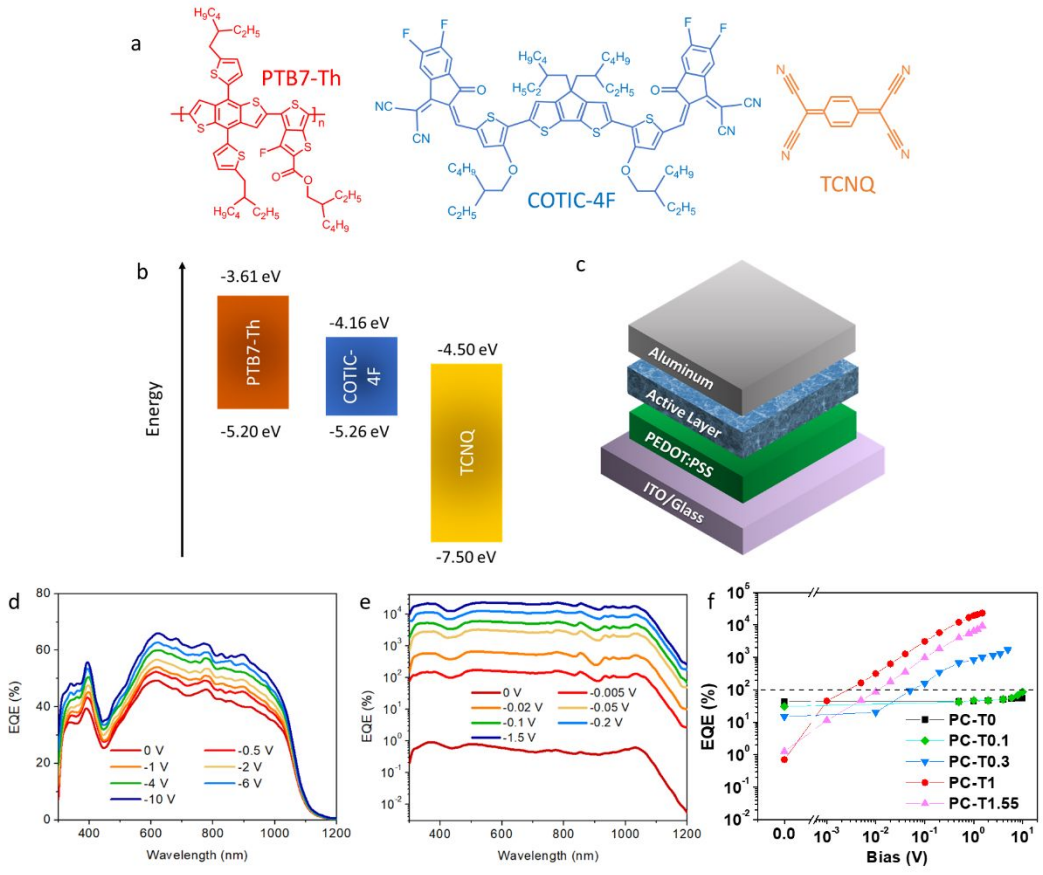

Fig. 1 (a) Chemical structures and (b) Energy levels of PTB7-Th, COTIC-4F and TCNQ. (c) Device configuration of the photodetectors. EQE profiles of (d) PC-T0 and (e) PC-T1 devices under various bias. (f) EQE as a function of the applied bias measured at monochromatic light of 550 nm for PC-T0, PC-T0.1, PC-T0.3, PC-T1 and PC-T1.55 devices.

PC-T0.1, PC-T0.3 and PC-T1.55 devices were also obtained (Fig. S1). The voltage-dependent EQE under 550 nm monochromatic light is summarized in Fig. 1f for all PC-Tx devices. From these data, one first notices that quantities of TCNQ tends to lead to a lower EQE under short-circuit conditions. It is possible that TCNQ molecules introduce traps states for photogenerated electrons with its deep lying lowest unoccupied molecular orbital (LUMO) level. These trap states can act as carrier recombination centers, decreasing the number of extractable photogenerated carriers.[26] For the case of saturated TCNQ (PC-T1.55), the EQE is slightly higher, possibly due to the higher tendency to aggregation of TCNQ and therefore some degree of alleviation of its charge trapping. In contrast for under-bias conditions, an opposite trend of EQE is observed from PC-T0 to PC-T1: the larger the quantity of TCNQ, the higher EQE can be achieved. As shown in Fig. 1f, the PC-T1 device shows $EQE_{(550\ nm)}$ of ~23300% at -1.5 V, while $EQE_{(550\ nm)}$ of the PC-T0.3 device is 1720% even at -5 V. For the PT-C0.1 device, the gain effect appears to be further weakened, with $EQE_{(550\ nm)}$ of only 86.7% and a maximum EQE of 98.1% achieved at 630 nm (Fig. S1b) under a large bias of -10 V. While the EQE obtained from the PC-T0.1 device is overall below 100%, the close-to-unity EQE of 98.1% compared to 55.8% of the PC-T0 device under the same bias (-10 V) still implies the presence of the gain effect in the PC-T0.1 device considering the losses from the photon absorption and charge recombination.

Apparently, the gain effect is related to the added TCNQ. When compared to previously reported PM OPDs based on trap-assisted charge injection mechanism, there exists such similarity where disproportionate ratios of the components in the active layer can be found. However, the much smaller gain-threshold voltage and the opposite trend of EQE as a function of the quantity of the trap-inducing materials suggest a different mechanism.[10,14] To obtain insights into the underlying dynamics, we sought to understand the effect of incorporating TCNQ on the charge transport properties of the devices. The focus is placed on the gain-absent PC-T0 and the highest gain PC-T1 devices. First, we assumed if the TCNQ-involved effect responsible for the observed gain occurs only in the bulk of the active layer, then changing the conditions at the interface between the active layer and electrode should not significantly alter the photoresponse behavior. Hence, modified PC-T1 devices were prepared, which feature a layer of Al-doped ZnO between the active layer and the Al top electrode (Fig. S2a). Surprisingly, the gain behavior was absent within a reasonable range of bias (Fig. S2b), and the achieved EQE at -10 V is close to that of the PC-T0 devices. This indicates that the assumption is not correct and a direct interaction between the Al electrode and the TCNQ on the surface of the active layer (interfacial TCNQ) is prerequisite for the gain effect to occur. As suggested by the Fourier-transform infrared (FT-IR) spectroscopy (Fig. S3a), Al-TCNQ complex may be formed at the metal/organic interface, which increases the work function of the electrode and lower the contact resistance for hole injection.[27–29] Therefore, we subsequently explored the change in the charge injection at the organic/metal interface by extracting the contact resistance (R_{ct}) using the transmission line method (TLM). It should be noted that in a BHJ system with such a narrow effective bandgap (~1.04 eV, defined as the difference between LUMO of the acceptor and highest occupied molecular orbital, or HOMO, of the donor), it is difficult to designate the measured current exclusively to the transport of holes or electrons due to the ambipolar nature of intrinsic organic semiconductors. Hence, a field-effect transistor (FET) architecture was employed for the TLM test. As such, the major contributing type of carriers can be modulated by the gate potential, allowing us to obtain R_{ct} values that reflect the interfacial charge transport for holes and electrons separately (Fig. 2a and 2b). To make the condition more relevant to the vertical photodetectors, top-contact device architecture was adopted, and Al was used as the electrode. By extrapolating the width-normalized total resistance ($R_{tot} \cdot W$) to the zero-channel length (L = 0), one can obtain the width-normalized contact resistance ($R_{ct} \cdot W$) according to the following equation:

$$R_{tot}W = \frac{V_D}{I_D}W = R_{ct}W + \frac{L}{\mu_{FET}C_i(V_G - V_T)}$$

where R_{tot} is the total resistance, V_D is the drain voltage, I_D is the drain current, R_{ct} is the contact resistance, μ_{FET} is the field-effect carrier mobility, C_i is the areal capacitance of the dielectric layer, V_G is the gate voltage and V_T is the threshold voltage. The calculated $R_{ct} \cdot W$ is 3.63×10^8 and 1.12×10^7 Ω·mm for the p-type operation of the FETs based on PC-T0 and PC-T1, respectively (Fig. 2c). It is noted that the devices based on PC-T1 are unable to be operated as n-type OFETs due to intensified electron trapping caused by TCNQ (Fig. S4),[30] and therefore, it is not possible to extract the $R_{ct} \cdot W$ under n-type transport for the PC-T1 to compare with the $R_{ct} \cdot W$ (3.90×10^7 Ω·mm) of the TCNQ-absent PC-T0. Nevertheless, the dramatic decrease of the $R_{ct} \cdot W$ by more than one order of magnitude for the p-type operation has confirmed the facilitated hole injection with TCNQ in presence. The difference of the work function of the pristine and TCNQ-treated Al films was obtained by scanning Kelvin probe microscopy (SKPM). The contact potential difference (CPD) is defined as:

$$e \cdot CPD = \Phi_{tip} - \Phi_{sample}$$

where e is the elementary charge, Φ_{tip} and Φ_{sample} are the work function of the measuring tip and the sample, respectively. The CPD profiles for the two types of Al films are shown in Fig. 2d and 3e, respectively. Line-scan profiles of the two samples (Fig. 2f) reveal that the CPD of the pristine Al film (CPD_{Al}) is 1.652±0.014 V, and that of the TCNQ-modified Al film ($CPD_{Al\text{-}TCNQ}$) is 0.988±0.010 V. Therefore, the change in work function upon modification of Al with TCNQ is about +0.664 eV according

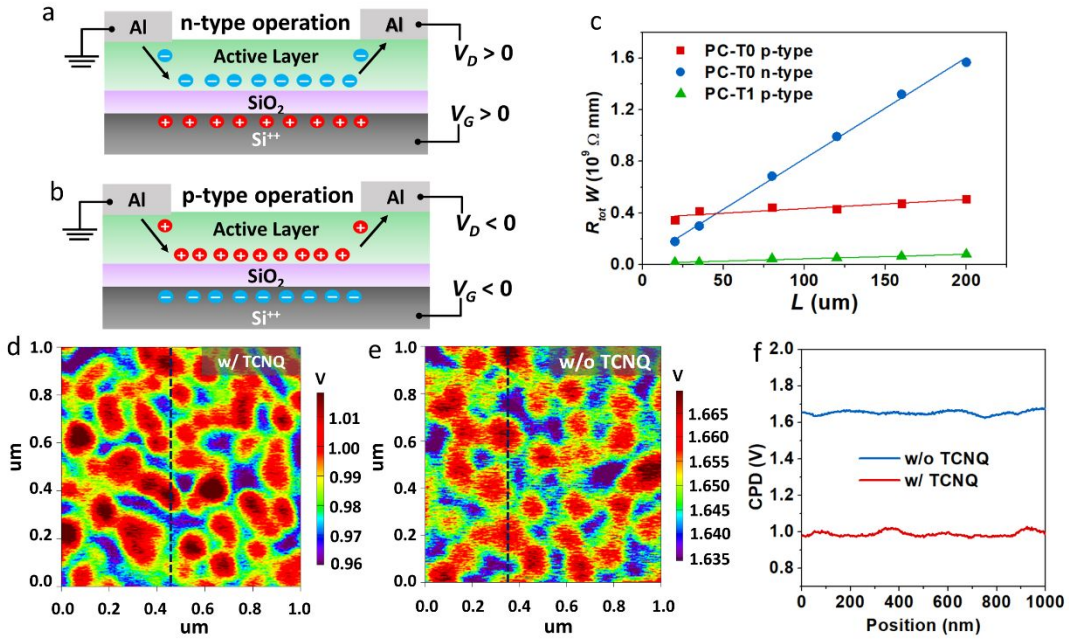

Fig. 2 Schematic of gate field-effect controlled charge transport allowing selectively probing the R_{ct} when the majority carriers are (a) electrons and (b) holes. (c) Plot of width-normalized total resistance (R_{tot} W) vs channel length (L) for the FETs with 1% and without TCNQ operated under n-type transport and p-type transport. 2D CPD images of the Al film (d) with and (e) without modification of TCNQ. (f) Line profiles of CPD for the samples in (d) at and (e).

to the equation:

$$\Delta\Phi = \Phi_{Al-TCNQ} - \Phi_{Al} = e\cdot(CPD_{Al} - CPD_{Al-TCNQ})$$

where $\Phi_{Al\text{-}TCNQ}$ and Φ_{Al} are the work function of the TCNQ-modified and pristine Al films, respectively. Thus, the increase in work function upon modification of TCNQ is behind the lowered contact resistance and the improved hole transport at the organic/metal interfaces. This agrees well with the trend of the *J-V* characteristics in the dark for all the photodetector devices (Fig. S5).

After revealing the effect of the TCNQ on the metal/organic interface, we further sought to understand the impact of TCNQ in the bulk of the active layer (bulk TCNQ). Modified PC-T0 devices were prepared, with the top electrode changed to MoO_x/Ag (Fig. S6a). The large work function of the MoO_x/Ag will enable efficient hole injection similar to the case of PC-T1. This type of devices is abbreviated as H-PC-T0 to present its dominant hole transport due to the charge selective electrodes. The EQE profile of the H-PC-T0 device (Fig. S6b) also shows EQE larger than 100%, which is, however, lower than that of the PC-T1 counterpart. This contrast implies that although the bulk TCNQ is not a determining factor as to whether the gain effect can be obtained, its existence contributes to a stronger gain effect. Single-carrier diodes with active layers of PC-T0 and PC-T1 were made to extract the electron and hole mobilities (Fig. S7). The hole and electron mobilities of PC-T0 devices were found to be $(2.12\pm0.32)\times10^{-4}$ and $(1.27\pm0.23)\times10^{-4}$ cm^2 $V^{-1}s^{-1}$. For PC-T1, the values were $(2.86\pm0.73)\times10^{-4}$ and $(1.93\pm1.61)\times10^{-6}$ cm^2 $V^{-1}s^{-1}$ for hole and electron, respectively. Considerable decrease of electron mobility is observed with PC-T1 devices. To examine whether such decrease is due to changes in film morphologies caused by TCNQ, we analyzed grazing-incidence wide-angle X-ray scattering (GIWAXS) data for both PC-T0 and PC-T1 films.[31] Both films adopt a face-on orientation for the main components of donor and acceptor materials (Fig. S8), and their differences in π-π stacking distances are insignificant (**Table S1**). It is noticed the coherence lenght (L_C) shows a degree of decrease for certain q_{xy} and q_z features, possibly due to the disruption from TCNQ, which however cannot be directly correlated to the observed change of vertical charge transport (detailed discussion in the SI). The similarity in overall ordering of the thin films is also consistent with the close Urbach energies of PC-T0 (64.6 meV) and PC-T1 (66.4 meV) (Fig. S9), indicating a similar level structural disorder.[32] The surface morphologies probed by atomic force microscopy (AFM) reveal a slight differece in surface roughness (Δrms ~1.638 nm) with similar film qualities and no drastic difference for PC-T0 and PC-T1 samples (Fig. S10). Thus, the decrease of electron mobility can be well rationalized by the energy landscape of the PC-T1, where electrons are energetically preferable to transfer from LUMO levels of the D-A blend to that of TCNQ. The small amount of TCNQ also makes it relatively morphologically isolated and difficult for uninterrupted electron transport, effectively lowering the electron mobilities.

With these results, we propose that the photocurrent gain originates from the imbalance between hole and electron transport, which, to a certain degree, may be similar to Si photoconductors.[33,34] The different schematics of photocurrent generation are shown for the devices with and without TCNQ, respectively. For the devices without TCNQ (Fig. 3a), the operation is that of a junction photodiode working in the

reverse bias region, where the photogenerated holes and electrons are collected with the externally applied bias and the built-in potential. The carriers contributing to the photocurrent are all from the photogeneration, and thus the EQE cannot exceed 100% considering the inevitable loss in absorption and recombination. For the devices with TCNQ (Fig. 3b), bulk TCNQ causes trapping of photogenerated electrons, which will induce extra holes to be injected due to charge neutrality, while interfacial TCNQ promotes hole injection by increasing the work function of the electrode, rather than by inducing strong band bending in previous reports.[35] Ultimately, the electron trapping and facile hole injection together lead to the net transfer of a large amount of charges from external circuit and manifests it as a strong photocurrent gain. It is worth noting that, considering the function of the Al-TCNQ complex in this gain mechanism, it is also possible that large work function electrodes (e.g., Ag/MoO_x or Au) can be readily used in combination with the bulk TCNQ to achieve high photocurrent gain.

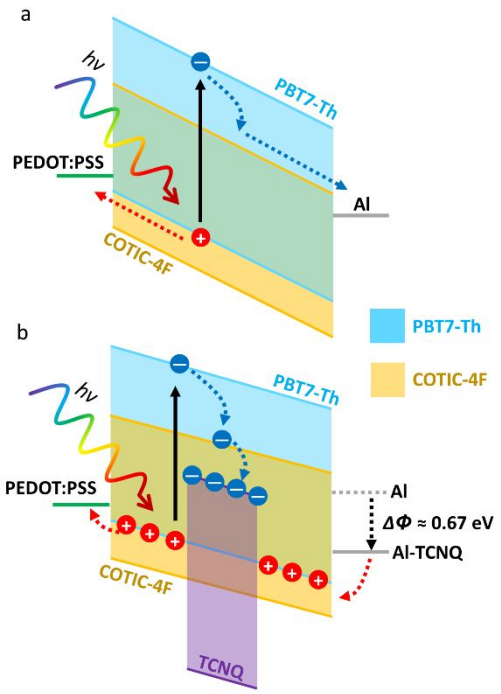

Fig. 3 A schematic of the photoresponse in the devices (a) with and (b) without TCNQ in the active layer under bias.

The photocurrent density (J_{ph}) as a function of light intensity (E) is plotted (Fig. 4a). The slopes of the linear fits in the logarithmic plot are close to unity. Hence, an approximate linear scaling of J_{ph} with light intensity is observed for all biases at lower light intensity. The linear region is followed by a sub-linear region typically observed in the photoconductors at higher light intensity, which is related to the photo-induced saturation of the traps states.[36] The EQE – light intensity characteristics are shown in Fig. 4b. Under weak light intensity, the photogeneration rate is low, and therefore, the extent of trap filling is low. There are enough traps available for the occurrence of the gain effect. As the photogeneration rate increases with more incident photons, more and more traps are filled by the photogenerated carriers. Ultimately, it leads to less prominent gain effect at higher light intensity. Since the photocurrent gain originates from the hindered transport of photogenerated electrons due to the presence of traps, EQE – light intensity characteristics can be well fitted with a photoconductive model:

$$EQE = \eta\left[\frac{1}{1+\left(E/E_0\right)^n}\right]$$

where η is a prefactor, representing the EQE at low light intensity, E_0 is the onset light intensity of trap saturation, and n is a fitting parameter.[37] The weak bias dependence of both n (0.71-0.77) and E_0 (63.6-70.5 uW/cm^2) suggests the trap filling is mainly dominated by photogeneration rather than the electric field strength. The linear dynamic range (LDR) can be estimated from the following equation:

$$LDR = 20 \times \log\frac{E_{upper}}{E_{lower}}(dB)$$

where E_{lower} and E_{upper} stand for the lower and upper limits of the light intensity at which the relationship between the device output and incident optical signal deviates linearity. According to the photoconductive model, a constant EQE is expected at light intensities much smaller than E_0. Therefore, E_{lower} can be estimated as the lowest detectable light intensity, namely the noise equivalent power (*NEP*) per unit area, which can be estimated from the measred noise current and EQE at low light intensity according to the following equation:

$$\frac{NEP}{A} = \frac{J_n}{EQE \cdot \frac{e\lambda}{hc}}$$

where A is the device area, J_n is the noise current density, e is the elementary charge, λ is the wavelength, h is Planck constant and c is the speed of light. Therefore, the lower detection limits are 8.46 × 10^{-11}, 5.04 × 10^{-11} and 1.07 × 10^{-10} W cm^{-2} under -0.1, -0.5 and -1.5 V, respectively. The LDR is estimated to be ~95 dB at -0.5 V, standing out favorably among other gain photodetectors that generally show a much narrow range of linear photoresponse, if not completely sub-linear photoresponse.[8,37–39]

The response speed can be evaluated by the rise time (t_r) and fall time (t_f), defined as the time needed for the photoresponse to occur between 10% and 90% of its steady-state photocurrent. Fig. 4c and 4d show the normalized transient response of a PC-T1 photodetector upon the introduction/removal of a 940 nm optical signal. The t_r and t_f are estimated to be 0.59 ms and 9.04 ms, respectively, which are much shorter than the typical human response time (250-950 ms to visual stimuli[40]). This result also compares favorably with many organic or hybrid gain photodetectors.[8,12,19,36,41,42]

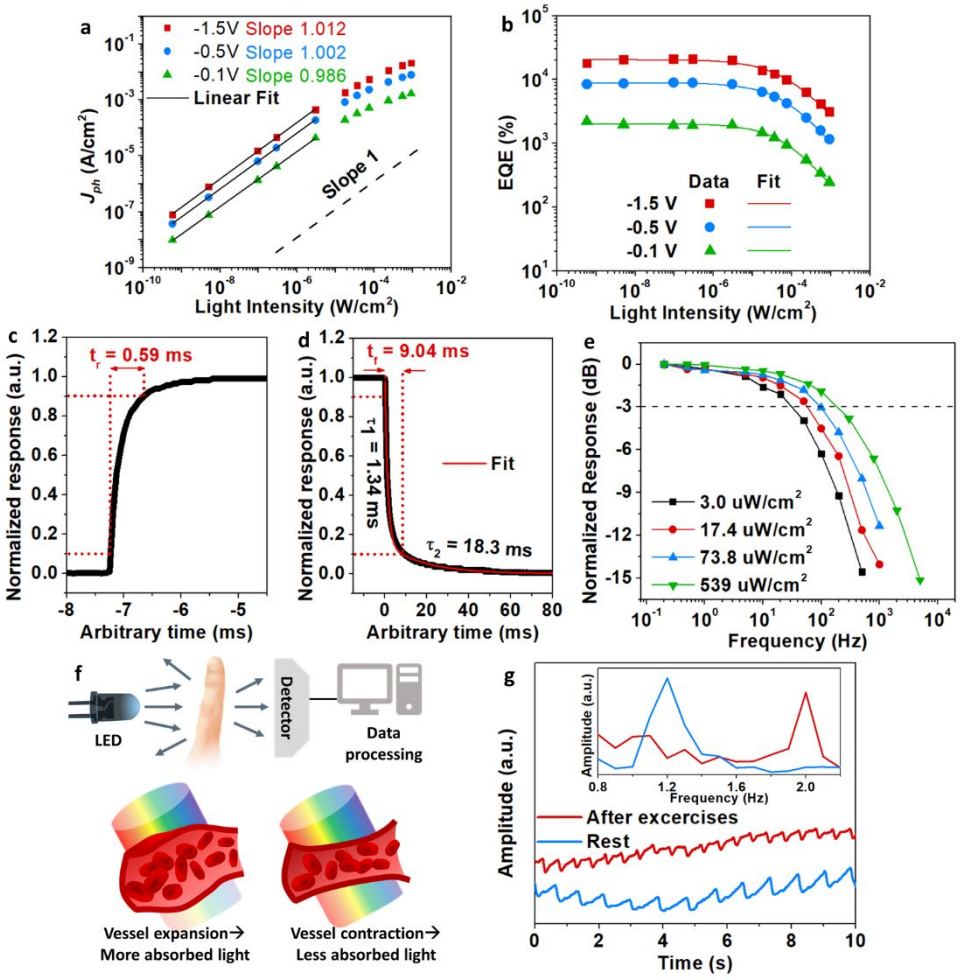

Fig. 4 (a) Photocurrent density - light intensity and (b) EQE (@940 nm) characteristics under different biases. The the horizontal dashed lines indicate the area-normalized noise current under each bias. Transient (c) rise and (d) decay curves upon application/removal of 940 nm light (~539 uW/cm^2). (e) Normalized response versus frequency under different light intensities. (f) Test setups and working principles of PPG. (g) Pulse signal versus time obtained from the PGG measurement. The inset is the fast-Fourier transform of the signal.

Exponential fitting of the decay curve finds a faster component of time constant τ_1 = 1.34 ms and a slower component of τ_2 = 18.3 ms, implying multiple pathways for recombination. Deep electron traps induced by LUMO level of TCNQ may have longer trapping release time that cause the slower component in the decay characteristics.[10] The cutoff frequency (f_{3dB}) was obtained by measuring phototransient response at different modulation frequencies. The f_{3dB} ranges from 30 to 180 Hz at the light intensities from 3 to 539 uW/cm^2 (Fig. 4e). At lower light intensities, the degree of trap-filling is lower, and thus rendering the transient behavior more dominated by the slower process related to deep traps. Regardless, the speed is still fast enough for the usually involved weak light intensity (<10^{-1} mW/cm^2) in medical imaging and photoplethysmography (PPG) applications.[7]

A simple PPG-based heart rate (HR) measurement was conducted to showcase the capability of the photodetectors in real-time monitoring. In a typical PPG test, a photodetector device collects the light signal that has been reflected/scattered by the human body part (Fig. 4f). Due to the volume change of the blood vessels and the density fluctuation of the light-absorbing blood hemoglobin during cardiac cycles, the intensity of the light that a nearby photodetector receives is modulated by the contraction and expansion of the vessels, which can lead to a small 'AC' signal reflecting the heartbeat.[5] The light scattered by a finger was collected by the photodetector and the real-time signal output of the photodetector was collected for a volunteer under his resting and after-exercise conditions (Fig. 4g). Fourier transform of the signals (inset of Fig. 4g) reveals the frequency of the pulse to be about 1.2 and 2 Hz for the two conditions, respectively. These are translated into HR of 72 and 120 /min.

Additionally, we prepared devices with active layers containing 1% TCNQ based on another two D-A blends (Fig. S11a). A small-molecule acceptor, CO1-4Cl,[43] was coupled with PTB7-Th, and polymer donor poly(3-hexylthiophene), P3HT, was coupled with COTIC-4F. The PTB7-Th:CO1-4Cl:TCNQ system shows EQE up to about 3500% (Fig. S11b), while the P3HT:COTIC-4F:TCNQ device delivers EQE between 100% and 200% (Fig. S11c). We noticed that the PTB7-Th:CO1-4Cl system

without TCNQ can achive EQE values close to that of PC-T0 (Fig. 1d). Since under large bias, the non-geminate recombination of the free carriers is minimized, such close EQE insinuates their similarly favorable photon capture and photogeneration. Hence, the performance difference in the TCNQ-present counterparts may be more related to difference in the electron trapping. Differently for the P3HT:COTIC-4F blend, the much lower EQE (<10%) compared to the other two systems in the case without TCNQ suggests inferior photogeneration from this particular D-A combination in the first place, unfavorable for achieving appealing photocurrent gain since the ultimate gain is positively related to the first step of photogeneration in the film.[36] Understandably, the performance for these two blends was obtained without extensive processing optimizations for the specific blends, and the differences in blend crystallinity, phase separation, and energy levels may lead to considerable variations in photogeneration rate, charge mobility, trap density, etc., ultimately manifesting a large difference in photoresponse. Regardless, this initial result suggests the universality of the approach to introduce photocurrent gain to organic BHJ systems. The performance difference also preliminarily indicates the possible features of BHJ systems that may potentially lead to promising photoresponse under the gain mechanism in this work. Further detailed structure-property studies are needed to deepen the understanding of this topic.

Conclusions

In summary, by introducing a small quantity of TCNQ into the BHJ blend, gain OPDs have been obtained, which can deliver not only large EQE over 10^4 % at low operation voltages (0.5-1.5 V), but also a wide span of spectral response (300 – 1200 nm). The simultaneously achieved large photoresponse, low driving voltage, wideband sensitivity and fast response set this work apart from existing gain OPDs. The origin of the observed large photocurrent gain is ascribed to the metal-TCNQ interaction and electron trapping by bulk TCNQ. These effects essentially convert the device behavior from that of a regular junction photodiode to a photoconductor with excessive trapping sites for electrons. With the strategy readily applicable to other D-A blends, we expect the presented approach to benefit from the large pool of organic BHJ systems, providing further improved and tunable photosensing performance with additional optimization.

Acknowledgements

This work is financially supported by the Mitsubishi Chemical Center for Advanced Materials. J. L. is grateful to the Center for Advanced Soft Electronics under the Global Frontier Research Program of the Ministry of Science, ICT & Future Planning, Korea (Grant Code No. 2011-0031628) for financial support. The GIWAXS measurement used resources of the Advanced Light Source, which is a DOE Office of Science User Facility under Contract No. DE-AC02-05CH11231. The authors are grateful to Dr. Alexander A. Mikhailovsky, Dr. Viktor V. Brus, Dr. Akchheta Karki, Zhifang Du and Ziyue Zhu for helpful discussion. Institutional review board (IRB) oversight is not required for this project as determined by the Human Subjects Committee (HSC) at University of California, Santa Barbara.

Conflicts of interest

There are no conflicts to declare.

Notes and references

1 G.-H. Lee, H. Moon, H. Kim, G. H. Lee, W. Kwon, S. Yoo, D. Myung, S. H. Yun, Z. Bao and S. K. Hahn, *Nature Reviews Materials*, 2020, **5**, 149–165.
2 X. Gong, M. Tong, Y. Xia, W. Cai, J. S. Moon, Y. Cao, G. Yu, C.-L. Shieh, B. Nilsson and A. J. Heeger, *Science*, 2009, **325**, 1665–1667.
3 J. Clark and G. Lanzani, *Nature Photonics*, 2010, **4**, 438–446.
4 P. C. Y. Chow and T. Someya, *Advanced Materials*, 2020, **32**, 1902045.
5 C. M. Lochner, Y. Khan, A. Pierre and A. C. Arias, *Nature Communications*, 2014, **5**, 1–7.
6 L. Dou, Y. Liu, Z. Hong, G. Li and Y. Yang, *Chem. Rev.*, 2015, **115**, 12633–12665.
7 X. Liu, Y. Lin, Y. Liao, J. Wu and Y. Zheng, *Journal of Materials Chemistry C*, 2018, **6**, 3499–3513.
8 Y.-L. Wu, K. Fukuda, T. Yokota and T. Someya, *Advanced Materials*, 2019, **31**, 1903687.
9 H.-Y. Chen, M. K. F. Lo, G. Yang, H. G. Monbouquette and Y. Yang, *Nature Nanotechnology*, 2008, **3**, 543–547.
10 F. Guo, B. Yang, Y. Yuan, Z. Xiao, Q. Dong, Y. Bi and J. Huang, *Nature Nanotechnology*, 2012, **7**, 798–802.
11 J. Miao, F. Zhang, M. Du, W. Wang and Y. Fang, *Advanced Optical Materials*, 2018, **6**, 1800001.
12 F. Tang, C. Wang, Q. Chen, J. Lai, W. Wang, F. Zhang and L. Chen, *Appl. Phys. Lett.*, 2018, **113**, 043303.
13 D. K. Neethipathi, H. S. Ryu, M. S. Jang, S. Yoon, K. M. Sim, H. Y. Woo and D. S. Chung, *ACS Appl. Mater. Interfaces*, 2019, **11**, 21211–21217.
14 L. Li, F. Zhang, J. Wang, Q. An, Q. Sun, W. Wang, J. Zhang and F. Teng, *Scientific Reports*, 2015, **5**, 9181.
15 S.-T. Chuang, S.-C. Chien and F.-C. Chen, *Applied Physics Letters*, 2012, **100**, 013309.
16 W. T. Hammond and J. Xue, *Appl. Phys. Lett.*, 2010, **97**, 073302.
17 R. Dong, C. Bi, Q. Dong, F. Guo, Y. Yuan, Y. Fang, Z. Xiao and J. Huang, *Advanced Optical Materials*, 2014, **2**, 549–554.
18 Z. Zhao, J. Wang, C. Xu, K. Yang, F. Zhao, K. Wang, X. Zhang and F. Zhang, *J. Phys. Chem. Lett.*, 2020, **11**, 366–373.
19 L. Li, F. Zhang, W. Wang, Y. Fang and J. Huang, *Physical Chemistry Chemical Physics*, 2015, **17**, 30712–30720.
20 W. Wang, F. Zhang, M. Du, L. Li, M. Zhang, K. Wang, Y. Wang, B. Hu, Y. Fang and J. Huang, *Nano Letters*, 2017, **17**, 1995–2002.
21 L. Li, F. Zhang, W. Wang, Q. An, J. Wang, Q. Sun and M. Zhang, *ACS Appl. Mater. Interfaces*, 2015, **7**, 5890–5897.
22 K.-J. Baeg, M. Binda, D. Natali, M. Caironi and Y.-Y. Noh, *Advanced Materials*, 2013, **25**, 4267–4295.
23 J. Lee, S.-J. Ko, H. Lee, J. Huang, Z. Zhu, M. Seifrid, J. Vollbrecht, V. V. Brus, A. Karki, H. Wang, K. Cho, T.-Q. Nguyen and G. C. Bazan, *ACS Energy Lett.*, 2019, **4**, 1401–1409.

24 J. Miao and F. Zhang, *Laser & Photonics Reviews*, 2019, **13**, 1800204.
25 R. Nie, X. Deng, L. Feng, G. Hu, Y. Wang, G. Yu and J. Xu, *Small*, 2017, **13**, 1603260.
26 L. Kaake, X.-D. Dang, W. L. Leong, Y. Zhang, A. Heeger and T.-Q. Nguyen, *Advanced Materials*, 2013, **25**, 1706–1712.
27 M. Mohammadtaheri, R. Ramanathan and V. Bansal, *Catalysis Today*, 2016, **278**, 319–329.
28 N. Koch, S. Duhm, J. P. Rabe, A. Vollmer and R. L. Johnson, *Phys. Rev. Lett.*, 2005, **95**, 237601.
29 C. Di, G. Yu, Y. Liu, X. Xu, D. Wei, Y. Song, Y. Sun, Y. Wang, D. Zhu, J. Liu, X. Liu and D. Wu, *J. Am. Chem. Soc.*, 2006, **128**, 16418–16419.
30 M. J. Ford, M. Wang, H. Phan, T.-Q. Nguyen and G. C. Bazan, *Advanced Functional Materials*, 2016, **26**, 4472–4480.
31 J. Lee, S.-J. Ko, M. Seifrid, H. Lee, B. R. Luginbuhl, A. Karki, M. Ford, K. Rosenthal, K. Cho, T.-Q. Nguyen and G. C. Bazan, *Advanced Energy Materials*, 2018, **8**, 1801212.
32 N. A. Ran, J. A. Love, C. J. Takacs, A. Sadhanala, J. K. Beavers, S. D. Collins, Y. Huang, M. Wang, R. H. Friend, G. C. Bazan and T.-Q. Nguyen, *Advanced Materials*, 2016, **28**, 1482–1488.
33 S. M. Sze, Kwok K. Ng, *Physics of Semiconductor Devices*, John Wiley & Sons, Inc., Hoboken, NJ **2007**.
34 B. E. A. Saleh, M. C. Teich, *Fundamentals of Photonics*, John Wiley & Sons, Inc., Hoboken, NJ **1991**.
35 D. Zhang, C. Liu, K. Li, W. Guo, F. Gao, J. Zhou, X. Zhang and S. Ruan, *Advanced Optical Materials*, 2018, **6**, 1701189.
36 C. Soci, A. Zhang, B. Xiang, S. A. Dayeh, D. P. R. Aplin, J. Park, X. Y. Bao, Y. H. Lo and D. Wang, *Nano Lett.*, 2007, **7**, 1003–1009.
37 X. Zhou, D. Yang, D. Ma, A. Vadim, T. Ahamad and S. M. Alshehri, *Advanced Functional Materials*, 2016, **26**, 6619–6626.
38 J. Gao and F. A. Hegmann, *Appl. Phys. Lett.*, 2008, **93**, 223306.
39 Q. Cui, Y. Hu, C. Zhou, F. Teng, J. Huang, A. Zhugayevych, S. Tretiak, T.-Q. Nguyen and G. C. Bazan, *Advanced Functional Materials*, 2018, **28**, 1702073.
40 S. Thorpe, D. Fize and C. Marlot, 1996, **381**, 3.
41 Y. Lee, J. Kwon, E. Hwang, C.-H. Ra, W. J. Yoo, J.-H. Ahn, J. H. Park and J. H. Cho, *Advanced Materials*, 2015, **27**, 41–46.
42 Z. Sun, Z. Liu, J. Li, G. Tai, S.-P. Lau and F. Yan, *Advanced Materials*, 2012, **24**, 5878–5883.
43 J. Huang, J. Lee, J. Vollbrecht, V. V. Brus, A. L. Dixon, D. X. Cao, Z. Zhu, Z. Du, H. Wang, K. Cho, G. C. Bazan and T.-Q. Nguyen, *Advanced Materials*, 2020, **32**, 1906027.